Intellectual disability risk gene RFX4 regulates cortical neurogenesis by restraining neuronal differentiation

Julianna J. Determan[1], Gareth Chapman[1], Sydney R. Crump[1], Faiza Batool[1], Sofia Malik[1], Taranjit S. Gujral[2], William Buchser[3,4], Caleb Valentine[3,4], Serena Elia[3,4], Monica Sentmanat[5], Xiaoxia Cui[4,5], Haley Jetter[6], and Kristen L. Kroll[1*]

1. Department of Developmental Biology, Washington University School of Medicine, St. Louis, MO 63110
2. Human Biology Division, Fred Hutchinson Cancer Center, Seattle, WA 98109
3. FIVE @ McDonnell Genome Institute, Washington University School of Medicine, St. Louis, MO 63110
4. Department of Genetics, Washington University School of Medicine, St. Louis, MO 63110
5. The Genome Engineering & Stem Cell Center (GESC@MGI), Washington University School of Medicine, St. Louis, MO 63110
6. Department of Pathology and Immunology, Washington University School of Medicine, St. Louis, MO 63110

[*]Corresponding author: kkroll@wustl.edu

Abstract

Despite the recent identification of RFX4 as a neurodevelopmental disorder risk gene, its role in cortical development remained unclear. Here, we identified both shared and lineage-specific RFX4 requirements for human cortical development using new human stem cell models of deficiency and pathogenic mutation. We found that RFX4 restrains neurogenesis by acting cooperatively with NOTCH signaling, specifically repressing pro-neuronal and synaptic gene expression in neural progenitors. We also determined that genome-wide binding of RFX3, another neurodevelopmental disorder risk gene, depends upon RFX4 to regulate synaptic gene expression. Furthermore, we identified lineage-specific functions for RFX4 in regulating proliferation during cortical inhibitory neuron development. Ultimately, we demonstrated that RFX4 deficiency persistently dysregulates neuronal gene expression through neuronal differentiation and disrupts cortical neuron stratification in organoid models. These consequences were absent in neurons generated by direct differentiation, confirming that neuronal phenotypes resulted from unconstrained neurogenesis. Finally, we modeled pathogenic missense mutation of the RFX4 DNA-binding domain. While this mutation strongly reduced DNA binding, it dysregulated synaptic gene expression distinctly from our deficiency models, supporting pathogenic mechanisms distinct from haploinsufficiency. Together, this work identified both shared and lineage-specific requirements for RFX4 during cortical development, building a necessary foundation for elucidating the etiology of RFX4-associated disorders.

Introduction

Development of the human cerebral cortex is a highly regulated process, with disruptions contributing to the etiology of neurodevelopmental disorders (NDDs) including intellectual disability (ID) and autism spectrum disorder (ASD) (Lui et al. 2011; Albert et al. 2017; Cadwell et al. 2019). A central hypothesis for the neuronal dysfunction underlying these NDDs involves imbalanced excitatory and inhibitory neuronal activity in the cerebral cortex (E/I imbalance) (Siegel-Ramsay et al. 2021; Hollestein et al. 2023) resulting from altered development and/or function of glutamatergic excitatory neurons (cEXs) and/or GABAergic inhibitory neurons (cINs). A major contributor to E/I imbalance is changes in the highly regulated process of cortical neurogenesis, a process by which proliferative neural progenitors differentiate into post-mitotic cortical neurons. While transcription factors (TFs) are major regulators of cortical neurogenesis (Cholfin and Rubenstein 2007; Villalba et al. 2021; Chapman et al. 2024; Vasan et al. 2025), with pathogenic mutations in these identified as frequent NDD contributors, it remains unclear how NDD-associated TF dysfunction differentially affects cEX versus cIN development to cause NDDs in humans. Thus, identifying both cell type-specific and -agnostic roles for NDD-associated TFs in regulating cortical neurogenesis is critical to understanding NDD etiology.

Towards this end, we modeled epigenetic regulation of human cIN development in prior work, deriving an atlas describing histone modification state changes accompanying cIN specification and differentiation from human pluripotent stem cells (hPSCs) (Chapman et al. 2024). This work identified Regulatory Factor X (RFX) 4 and RFX3 as key TFs regulating this process. As both *RFX3* and *RFX4* were also recently identified as NDD risk genes, with pathogenic mutations associated with global developmental delay, epilepsy, and ASD (Harris et al. 2021), these observations merited further study. Furthermore, while RFX3 is broadly expressed during human cortical development and included in multi-gene deletions that contribute to 9p deletion syndrome (Banerjee et al. 2019; Ajami et al. 2023; Wang et al. 2025), RFX4 expression is largely restricted to neural progenitors (Wang et al. 2025), suggesting a distinct role for RFX4 in regulating cortical neurogenesis.

RFX4 was initially identified as a gene involved in ciliogenesis (Ashique et al. 2009), while work in murine Rfx4 knockout (KO) models demonstrated Rfx4's necessity for proper brain development as homozygous (HOM) KO caused lethality by embryonic day 18.5 (Blackshear et al. 2003; Ashique et al. 2009; Xu et al. 2018). Rfx4 heterozygous (HET) knockdown animal models exhibited altered dorsal-ventral brain patterning associated with dysregulation of WNT, BMP, and SHH signaling (Zhang et al. 2006; Zhang et al. 2007; Ashique et al. 2009; Sedykh et al. 2018). More recently, studies using hPSC models have provided conflicting evidence for the role of RFX4 in cortical neurogenesis, suggesting that RFX4 overexpression could either produce a more homogenous neuronal progenitor population (Joung et al. 2023) or instead induce neuronal differentiation (Choi et al. 2024). Therefore, systematically defining the role RFX4 plays in regulating human cortical neurogenesis across cEX and cIN development is a necessary precursor to defining how pathogenic RFX4 mutations may alter cortical neurogenesis to disrupt E/I balance and contribute to NDDs.

Here, we used hPSC models with RFX4 loss of function (LOF) mutation to demonstrate that RFX4 LOF triggers dose-dependent precocious neurogenesis during both cIN and cEX development, ultimately causing deficits in cortical neuron layer stratification in organoids. We derived data for endogenous RFX4 binding, demonstrating that RFX4 commonly represses the expression of pro-neuronal and synaptic genes during both cEX and cIN development, while also activating proliferative gene expression, specifically in medial ganglionic eminence-like progenitors during cIN development. We further demonstrated that regulation of cortical neurogenesis by RFX4 involves both functional interplay with NOTCH signaling and with RFX3-mediated activation of neuronal gene expression. Finally, we modeled a patient specific missense mutation in the RFX4 DNA binding domain, demonstrating that this causes a dramatic loss of

RFX4 genome binding, but results in unique transcriptomic dysregulation and cellular phenotypes. Together, this defines the requirements for RFX4 and underlying mechanisms in regulating cortical neurogenesis and demonstrates that the etiology of RFX4-associated NDDs is more complex than haploinsufficiency-related LOF, as previously hypothesized. These findings provide a foundation for elucidating the basis of *RFX4* variant pathogenicity and targeting these mechanisms for reversal to ameliorate NDD-related consequences.

Results

Loss of RFX4 causes dosage-dependent induction of cortical neurogenesis

To characterize the effects of RFX4 loss of function (LOF) on human cortical development, we developed human pluripotent stem cell (hPSC) models with heterozygous (HET) or homozygous (HOM) RFX4 gene disruption (Fig. 1a, Supplementary Fig. S1a). Using our established protocols, we specified these hPSCs into neuronal progenitors (NPCs) with a dorsal (D-) or ventral (V-) telencephalic character (Fig. 1b). We then tested the validity of our LOF models in D-NPCs, confirming a ~60% and >90% loss of both RFX4 mRNA and protein in the HET and HOM models, respectively (Supplementary Fig. S1b-c). We next assessed how RFX4 deficiency changed neurosphere outgrowth during D-NPC and V-NPC specification, observing a significant reduction of outgrowth from both V-NPC (Fig. 1c-d) and D-NPC neurospheres (Fig. 1f-g). Interestingly, while neurosphere size was reduced during V-NPC specification (Fig. 1e), it was not significantly affected by RFX4 LOF during D-NPC specification (Fig. 1h), suggesting lineage specific roles for RFX4.

To further investigate lineage-specific RFX4 requirements, we performed RNA-sequencing in WT versus HOM D-NPCs and V-NPCs, highlighting both shared effects of RFX4 LOF and transcriptomic differences between the WT versus HOM D-NPC and V-NPC comparisons (Fig. 1i). We identified similar numbers of differentially expressed genes (DEGs) between WT and HOM D-NPCs (2,718) and HOM V-NPCs (2,456), respectively, with ~50% of DEGs upregulated upon RFX4 LOF (Fig. 1j, Supplementary Data 1). Notably, DEGs downregulated in both HOM D-NPCs and V-NPCs were enriched predominantly for genes involved in early developmental processes (Fig. 1k, Supplementary Data 2), while genes jointly upregulated upon RFX4 LOF were instead enriched for ‘synaptic signaling’ genes (Fig. 1l, Supplementary Data 2). Together, this work suggested that RFX4 may regulate the onset of neuronal differentiation similarly in both D-NPCs and V-NPCs.

We next validated altered expression of 10 upregulated (Fig. 1m-n) and 10 downregulated (Supplementary Fig. S1d-e) DEGs, using RT-qPCR in WT, HET, and HOM D- and V-NPCs and confirming that RFX4 LOF caused dosage-dependent changes in expression of these genes (Fig. 1m-n, Supplementary Fig. S1d-e). We further validated these findings by assessing the fraction of cells expressing ASCL1, a neurogenesis-promoting bHLH transcription factor, finding dose-dependent increases in the ASCL1 immunopositive cell fraction upon RFX4 LOF in both V-NPCs and D-NPCs (Fig. 1o-p). The proportion of DCX positive cells, a protein essential for neuronal migration, was likewise increased in both HET and HOM D-NPCs (Supplementary Fig. S1f). By contrast, we found that the proportion of cells immunopositive for the early-born neuron marker TBR1 was unaltered in D-NPCs (Supplementary Fig. S1g). Furthermore, while V-NPCs exhibited decreased proliferation, proliferation remained unchanged in D-NPCs (Supplementary Fig. S1h-i), supporting lineage-specific requirements for RFX4. Ultimately, these results indicated that RFX4 LOF triggers dosage-dependent neurogenesis, while also highlighting lineage-specific RFX4 requirements.

Interestingly, these results appeared inconsistent with a previous publication, which concluded that RFX4 overexpression (OE) promotes neuronal differentiation. Therefore, we tested whether RFX4 OE alone was sufficient to induce neuronal differentiation (Supplementary Fig. S2a). After confirming RFX4 OE (Supplementary Fig. S2b), we assessed expression levels of multiple neuronal genes by RT-qPCR, finding no significant increases (Supplementary Fig. S2c). Likewise, RFX4 OE was insufficient to induce the expression of either the early neuronal marker TUJ1 or ASCL1 (Supplementary Fig. S2d-e) or to change the proportion of cells immunopositive for pluripotency markers (Supplementary Fig. S2f-g). Together, these results further supported our hypothesis that RFX4 is required to regulate cortical neurogenesis by restraining premature neuronal differentiation, while demonstrating that RFX4 OE alone is insufficient to induce neurogenesis.

RFX4 directly restrains the onset of neuronal and synaptic gene expression

To identify genes directly regulated by RFX4, we defined endogenous RFX4 genome-wide binding using CUT&Tag, confirming an almost complete loss of RFX4 genome-wide binding in HOM D-NPCs (Fig. 2a). We analyzed the quality of these data by footprinting, identifying a footprint under RFX4 bound peaks in WT D-NPCs corresponding with a canonical RFX transcription factor binding site (TFBS) that was lost in HOM D-NPCs (Supplementary Fig. S3a). We further compared our endogenous RFX4 binding data to previously published chromatin immunoprecipitation (ChIP) data obtained by overexpressing epitope-tagged RFX4, finding over 12,000 binding sites specific to endogenous RFX4 (Supplementary Fig. S3b). Finally, we used a deep learning model to analyze the sequence syntax present at RFX4 bound peaks, demonstrating that the presence of an RFX TFBS was highly correlated with sites of RFX4 binding (Supplementary Fig. S3c). This work therefore identified the endogenous binding profile for RFX4 during human cortical development, confirming both the data validity and quality.

We next generated similar genome-wide binding data for RFX4 in WT versus HOM V-NPCs (Fig. 2b), identifying both D-NPC and V-NPC shared and lineage-specific RFX4 binding sites (Supplementary Fig. S3d). We associated RFX4 peaks with their nearest transcription start site (TSS) to identify RFX4 bound genes; we then defined which of these were also RFX4 DEGs (bound-DEGs) in D-NPCs and V-NPCs, finding substantial RFX4 binding near promoters and introns of bound-DEGs (Supplementary Fig. S3e-j). Bound-DEGs upregulated upon RFX4 LOF in both D-NPCs and V-NPCs were enriched for neuronal and synaptic genes (Fig. 2c-d, Supplementary Data 3), supporting a role for RFX4-mediated repression in regulating neurogenesis. By contrast, bound-DEGs downregulated upon RFX4 LOF uniquely in V-NPCs were associated with cell proliferation (Fig. 2e, Supplementary Data 3), consistent with our previous finding of reduced proliferation in HOM V-NPCs. These results suggest that while RFX4 has lineage-specific functions, it broadly represses neuronal and synaptic gene expression in both D-NPCs and V-NPCs.

As our work above highlighted shared cellular phenotypes across NPC lineages were more severe during D-NPC specification (Fig. 1p), we next focused on understanding RFX4's regulatory function in D-NPCs. We found that binding sites that were significantly lost upon RFX4 LOF (>2 fold, pValue<0.05) and were associated with DEGs (Supplementary Data 4) were enriched for RFX motifs and TEAD, homeodomain, and SOX family TFBSs (Fig. 2f, Supplementary Data 5), reminiscent of predictions made by our deep learning model (Supplementary Data 4). We focused on assessing potential interplay between RFX4 and TEAD1, given the latter's established role in neurogenesis and its upregulation upon RFX4 LOF (Mukhtar et al. 2020; Perry et al. 2025) (Supplementary Data 1), defining genome-wide TEAD1 binding in D-NPCs. This analysis showed minimal changes in TEAD1 binding upon RFX4 LOF (Supplementary Data 4), but defined sites co-bound by both TEAD1 and RFX4 in D-NPCs. These included sites associated with genes involved in WNT and NOTCH signaling, congruent with a potential role for RFX4 and TEAD1 in cooperatively regulating genes critical for NPC maintenance.

To identify a subset of key RFX4 direct targets for further experimental validation, we next focused on RFX4 bound sites that were both associated with a DEG and contained an RFX4 TFBS (Fig. 2g), finding that this DEG subset was enriched for synapse-associated genes upregulated upon RFX4 LOF (e.g. *SYT5*, *CAMK2A*; Fig. 2h-i, Supplementary Data 3). We cloned a set of RFX4 putative cis-regulatory elements (CREs) associated with these bound-DEGs into a luciferase reporter construct (Fig. 2j), finding that luciferase expression driven by a majority of these putative CREs increased significantly upon RFX4 LOF in D-NPCs (Fig. 2k). Together, this work confirmed RFX4's ability to repress gene expression at these sites, identifying new requirements for RFX4-mediated transcriptional repression of synaptic gene expression during cortical neurogenesis.

RFX4 regulates the onset of cortical neurogenesis downstream of NOTCH signaling

Our findings of TFBS co-enrichment at RFX4 bound sites above suggested functional interplay with other factors and/or signaling pathways in regulating human cortical neurogenesis. Therefore, to identify chemical modifiers of RFX4 LOF phenotypes, we performed an unbiased drug screen in WT and HOM D-NPCs. This screen identified mechanisms of action (MoAs) that normalized the increased proportion of LOF D-NPCs expressing the neurogenic bHLH TF OLIG2 (Supplementary Data 6). Interestingly, significant hits included γ-secretase inhibitors; this was of particular interest as NOTCH signaling is blocked by γ-secretase inhibitors and restrains neurogenesis. Therefore, we assessed if NOTCH inhibition (using DAPT, Fig. 3a) phenocopied RFX4 LOF. Transcriptomic analysis highlighted distinct differences between DAPT-treated WT (WT-DAPT) and HOM D-NPCs (Fig. 3b, Supplementary Data 7), despite the observation that RFX4 expression was reduced upon DAPT-treatment of WT D-NPCs (Supplementary Fig. S4a). Specifically, we found a more substantial upregulation of neuronal and synaptic gene expression in WT-DAPT versus untreated HOM D-NPCs (Fig. 3c-d, Supplementary Data 1, 8), a phenomenon that was further exacerbated when HOM D-NPCs were also DAPT treated (HOM-DAPT) (Fig. 3e, Supplementary Fig. S4b). DAPT treatment caused a similar increase of the fraction of TBR1 immunopositive cells in both WT and HOM D-NPCs, while RFX4 LOF alone instead reduced the TBR1 immunopositive cell fraction (Fig. 3f); these data suggested that NOTCH inhibition is sufficient to promote terminal neuronal differentiation, while RFX4 LOF is not. Based upon these findings, we hypothesized that RFX4 acts downstream of NOTCH signaling to restrain initiation of cortical neurogenesis, in part by directly repressing the expression of neurogenic TFs including ASCL1 (Supplementary Fig. S4c).

We next assessed if changes in chromatin state unique to NOTCH inhibition could be used to identify TFs that could potentially co-function with RFX4 downstream of NOTCH signaling. Specifically, we assessed changes in the repressive modification histone 3 lysine 27 tri-methylation (H3K27me3) and primed enhancer marker histone 3 lysine 4 mono-methylation (H3K4me), observing substantive changes in H3K4me (Supplementary Fig. S4d-e) but minimal changes in H3K27me3 (Supplementary Fig. S4f-g) upon either RFX4 LOF or DAPT treatment. Further analysis highlighted increased H3K4me association with synaptic and neuronal genes after either RFX4 LOF or DAPT treatment (Supplementary Data 8-9), which increased upon DAPT treatment of HOM D-NPCs (Fig. 3g, Supplementary Data 9). We also assessed H3K4me changes specific to DAPT treatment alone, finding that sites that lost H3K4me upon NOTCH inhibition in D-NPCs were enriched for high mobility group (HMG) TFBSs (Fig. 3h, Supplementary Data 10). Among HMG family TFs, SOX2 was most substantially and specifically downregulated upon NOTCH inhibition (Supplementary Data 1,7), suggesting that continued SOX2 expression upon RFX4 LOF could facilitate maintenance of NPC gene expression. To identify other TFs that could restrain terminal neuronal differentiation specifically in RFX4 LOF D-NPCs, we turned to our in-silico footprinting analysis, finding a HES TFBS footprint was gained upon RFX4 LOF (Supplementary Fig. S4h). Among this TF family, HES5 was most strongly downregulated specifically by NOTCH inhibition (Supplementary Data 1,7), suggesting that both SOX2 and HES5 function with RFX4 to regulate cortical neurogenesis downstream of NOTCH signaling.

To test potential functional interplay between these TFs during cortical neurogenesis, we performed siRNA knockdown (KD) of either SOX2 and/or HES5 in WT and HOM D-NPCs. SOX2 and HES5 levels were significantly reduced specifically in the presence of siRNAs targeting these genes, with a single siRNA targeting each gene selected for further study (siRNA 3; Fig. 3i-j, Supplementary Fig. S4i-k). Following either SOX2 or HES5 KD, RFX4 mRNA levels decreased significantly (Supplementary Fig. S4l), suggesting direct or indirect transcriptional regulatory control of RFX4 expression by SOX2 and HES5. SOX2 KD reduced neuronal marker expression similarly in both WT and HOM D-NPCs (Fig. 3kl, Supplementary Fig. S4m-o). However, HES5 KD caused differential effects in WT versus HOM D-NPCs (Fig. 3k-l, Supplementary Fig. S4m-o), promoting upregulation of the cortical deep layer neuron markers TBR1 and CTIP2 in WT but not HOM D-NPCs (Fig. 3k-l). These results demonstrate that, while SOX2 KD alters neuronal gene expression changes similarly regardless of RFX4 levels, TBR1 upregulation upon HES5 KD is hampered by RFX4 LOF, suggesting that RFX4 and HES5 function cooperatively to restrain neurogenesis and differentiation. Together, these results highlight a role for RFX4 in regulating the onset of cortical neurogenesis downstream of key NOTCH effectors, specifically by regulating the formation of early born, deep layer neurons in the developing cortex.

RFX3 binding is contingent on RFX4 but plays a unique neurodevelopmental role

Our work above highlighted a requirement for functional interplay between RFX4 and other TFs to restrain cortical neurogenesis. Given that RFX family TFs can both homo- and hetero-dimerize (Morotomi-Yano et al. 2002) and RFX3 deletion is also associated with NDDs (Banerjee et al. 2019; Ajami et al. 2023), it is plausible that RFX4 acts with other RFX TFs to co-regulate human cortical development. To assess this potential functional interplay, we first compared their expression, finding that both RFX3 and RFX4 expression peaked in NPCs, while only RFX3 expression persisted following neurogenesis (Fig. 4a). We next examined how RFX4 LOF affected RFX3's ability to bind DNA, finding a substantial loss of RFX3 genome-wide binding in HOM D-NPCs (Fig. 4b, Supplementary Data 11), particularly at cis-regulatory regions of neuronal and synaptic genes (Fig. 4c, Supplementary Fig. S5a, Supplementary Data 12). Furthermore, we identified RFX3 and RFX4 co-bound sites (Fig. 4d); these were associated with RFX4 DEGs, were enriched for RFX, TEAD, and SOX TFBSs (Fig. 4e, Supplementary Data 13), and were predominately involved in synapse development (Fig. 4f, Supplementary Data 12).

Together, these results indicate that RFX3 binding is contingent upon RFX4 expression and suggest that both RFX TFs play roles in direct regulation of synapse-related gene expression.

To assess if the RFX4-dependent RFX3 binding we observed above was reciprocal, we next generated hPSC models with homozygous RFX3 LOF (RFX3-HOM, Fig. 4g, Supplementary Fig. S5b) and validated loss of RFX3 expression in RFX3-HOM D-NPCs (Supplementary Fig. S5c-d). We assessed RFX3 genome-wide binding in WT and RFX3-HOM D-NPCs, demonstrating that RFX3 binding was enriched at gene promoters and was lost upon RFX3 LOF (Supplementary Fig. S5e-f, Supplementary Data 11). However, RFX3 LOF resulted in minimal alteration of RFX4 binding (Supplementary Fig. S5g), indicating that RFX4 genome-binding does not reciprocally depend upon RFX3. Additionally, RFX3 LOF resulted in unique cellular phenotypes; for example, unlike RFX4 LOF, RFX3 LOF caused no change in neurosphere size, outgrowth, or proliferative and neurogenic marker immunopositivity (Supplementary Fig. S5h-m), suggesting that RFX3, unlike RFX4, is not required to restrain cortical neurogenesis. Interestingly, transcriptomic analysis confirmed both distinct and shared gene expression changes upon either RFX3 LOF or RFX4 LOF (Fig. 4h, Supplementary Data 14). Specifically, LOF of each TF resulted in shared upregulation of apoptosis associated genes (Fig. 4i, red box, Supplementary Data 12) and shared downregulation of early neuronal genes (Fig. 4i, blue box, Supplementary Data 12). However, RFX3 LOF uniquely caused the downregulation of synapse-related genes, many of which were bound by RFX3 at promoters under WT conditions (Fig. 4j, Supplementary Fig. S5n-o, Supplementary Data 12). Many of these genes were instead upregulated by RFX4 LOF (Supplementary Data 12). These results highlight both shared and antagonistic roles for RFX3 and RFX4 during cortical neurogenesis, specifically in restraining synaptic gene expression, with RFX4 having a more substantial role in regulating this process.

Pathogenic *RFX4* missense mutation disrupts genome-wide binding, but has distinct effects from LOF on transcriptional regulation

As RFX4 was recently classified as an NDD risk gene with pathogenic mutations hypothesized to act by LOF (Harris et al. 2021), we next generated hPSC models heterozygous or homozygous for a pathogenic p.R79C missense mutation in the RFX4 DNA binding domain (R79C-HET and R79C-HOM, respectively; Fig. 5a, Supplementary Fig. S6a). Levels of RFX4 mRNA and protein were assessed in R79C-HET and R79C-HOM D-NPCs, highlighting substantially reduced RFX4 protein levels specifically in the R79C-HOM but not R79C-HET D-NPCs (Supplementary Fig. S6b-c); these data suggest that this mutation could disrupt the expression and/or protein stability of RFX4 and may alter its function. Consistent with pathogenic disruption of the DNA binding domain of RFX4, we found an almost complete loss of RFX4 genome-wide binding in R79C-HOM D-NPCs (Fig. 5b, Supplementary Fig. S6d, Supplementary Data 15). This occurred at similar locations and was associated with a loss of binding at many of the same genes defined in the LOF HOM D-NPCs (e.g. *DLG4* and *SCRN1*; Fig. 5c-e, Supplementary Data 16), suggestive of LOF as a potential mechanism of pathogenicity.

We next assessed transcriptomic changes in R79C-HOM versus WT D-NPCs, surprisingly finding substantially different DEGs in R79C-HOM versus LOF HOM versus matched control D-NPC data comparisons (Fig. 5f). Likewise, unlike the LOF model, R79C-HOM D-NPCs did not alter neurosphere outgrowth (Supplementary Fig. S6e-g). Further analysis identified many R79C-HOM specific DEGs (Supplementary Data 16), with predominant downregulation of neuronal and synaptic gene expression by contrast with HOM D-NPCs (Supplementary Data 1,16). We also identified a small set of shared DEGs with similarly dysregulated expression in both R79C-HOM and HOM D-NPCs (Fig. 5g); these shared downregulated DEGs were enriched for cell migration genes, while shared upregulated DEGs were instead enriched for early forebrain development genes (Fig. 5h, Supplementary Data 16). Together, these results highlight the unexpected finding that, while p.R79C pathogenic mutation disrupts genome-wide RFX4 binding like LOF, it causes distinct transcriptomic changes.

We next tested whether these transcriptional consequences were dependent upon homozygosity for the p.R79C mutation, finding that, unlike R79C-HOM, R79C-HET had minimal consequences on RFX4 genome-wide binding in D-NPCs (Fig. 5i, Supplementary Fig. S6h, Supplementary Data 15). We also examined a selection of DEGs that were differentially regulated in the R79C versus the LOF models, finding that both R79C-HET and R79C-HOM D-NPCs exhibited similar gene expression changes, while these differed from those seen in the HET and HOM LOF models (Fig. 5j). Furthermore, while LOF D-NPC models increased ASCL1 immunopositivity (Fig. 1p), neither R79C-HET or R79C-HOM D-NPCs did (Fig. 5k). Likewise, the KI67, FOXG1, and PAX6 immunopositive cell fractions were unchanged upon p.R79C mutation (Supplementary Fig. S6i-l). These findings demonstrate that, despite similarly reducing genome-wide binding, the p.R79C mutation disrupts transcriptional regulation distinctly from haploinsufficiency-related LOF.

RFX4 expression during neurogenesis is necessary for stratification of neuronal layers in cortical organoids

To examine the neuronal consequences of altered cortical neurogenesis resulting from RFX4 LOF, we next generated both cortical excitatory neurons (cEXs) by differentiating WT and HOM D-NPCs (Fig. 6a) and glutamatergic-like neurons (iGluts, Fig. 6b) by overexpressing Neurogenin-2 (NGN2), in WT and HOM hPSCs. As the generation of iGluts bypasses the formation of neuronal progenitors and RFX4 expression is temporally restricted to D-NPCs (Fig. 6c, Supplementary Fig. S7a-b), we tested whether transcriptomic changes caused by RFX4 LOF specifically in D-NPCs were detected in cEXs but not iGluts. We examined neuronal genes directly regulated by RFX4 in D-NPCs, observing continued upregulation of these genes in HOM cEXs, while HOM iGluts exhibited no consistent changes in expression of these genes (Fig. 6d). This assessment confirmed that neuronal consequences from RFX4 LOF require transit through a prior progenitor stage. To further examine the neuronal consequences of LOF, we performed RNA-sequencing in WT and HOM cEXs (Supplementary Fig. S7c) identifying consistently dysregulated DEGs common to both HOM D-NPCs and HOM cEXs (Supplementary Tabel 1,18). This analysis identified a persistent upregulation of TFs involved in neuronal specification (e.g. ASCL1, OLIG2, Fig. 6e-f, Supplementary Data 19) in both HOM D-NPCs and cEXs. These data confirm that transcriptomic disruptions caused by RFX4 LOF originate during D-NPC specification and persist through cEX differentiation, resulting in persistently elevated pro-neurogenesis gene expression in neurons that could potentially impact their later differentiation or maturation.

To examine if these disruptions altered the differentiation capacity, identity, and/or maturation of HOM cEXs, we next profiled expression of cortical layer markers and synaptic genes critical for glutamatergic neuron function, finding that many of these genes were downregulated in HOM cEXs (Fig. 6g). This was further supported by our RNA-sequencing data, which revealed the predominant downregulation of genes involved in the generation of neurons in HOM cEXs (Supplementary Data 19). As TBR1+ (deep cortical layer 6) neurons are the first subtype to be generated from D-NPCs during neurogenesis, we also examined the production of these neurons by immunofluorescence, finding that HOM cEX cultures failed to generate TBR1 immunopositive cells (Fig. 6h), although there was no significant difference in production of neurons expressing another deep layer 5/6 cortical neuron marker, CTIP2 (Fig. 6h). Finally, we examined synapse production in WT and HOM cEX cultures by examining the density of SYN1+ and PSD95+ puncta colocalized to TUJ1+ neurites, finding no alteration in the density of these synaptic markers in HOM cEXs (Fig. 6i). Together, these data suggest that, while these neurons initiate neurogenesis prematurely, some aspects of their later differentiation capacity are impaired.

The reduction of some neuronal marker expression in cEXs suggested that LOF effects on neurogenesis could persistently alter later neuronal differentiation and layering of the developing cortex. To examine this, we generated dorsal telencephalic patterned 3-D cortical organoids (D-ORGs, Fig. 6j). We first tested key neurogenesis-related phenotypes observed above in D-NPCs, focusing on approximately analogous D-ORG timepoint, day 30 (D30). Like our prior findings for D-NPCs, HOM D-ORGs exhibited precocious neurogenesis, as marked by an increased area expressing the newborn neuron marker TUJ1, with no change to the fraction of SOX2-expressing progenitors (Fig. 6k). This was congruent with a decreased KI67- and increased TBR1-immunopositive cell fraction (Supplementary Fig. S7d-e). We further detected an increased proportion of cells immunopositive for FOXG1, a cortical TF expressed throughout differentiation (Supplementary Fig. S7f), while neither the intermediate progenitor marker TBR2 (Supplementary Fig. S7g) nor ASCL1 were affected in organoid models (Supplementary Fig. S7h). Together these results demonstrate that RFX4 restrains cortical neurogenesis, while LOF causes precocious neurogenesis in both 2-D and 3-D models of cortical development.

As TBR1+ neuron production in cEX cultures was significantly reduced by RFX4 LOF, we further differentiated D-ORGs to day 60 (D60) to examine if cortical stratification into different neuronal subtypes/layers is similarly altered by RFX4 LOF. We found significant increases in the production of TBR1+ (Fig. 6l) and CTIP2+ (Fig. 6m) neurons upon RFX4 LOF and increases to the area expressing TUJ1 in D60 D-ORGs, with no change in the apoptosis marker Cleaved Caspase 3 (CC3) (Supplementary Fig. S7i). These results demonstrate that the increased production of early-born neurons persists to affect 3-D organoid cortical neuron layering. Together, these results support a progenitor-specific requirement for RFX4 to restrain cortical neurogenesis and differentiation, with its disruption causing persistent effects in neuron differentiation and stratification into layers in these hPSC-based models of human cortical development.

Discussion

In this work, we derived new hPSC models and used these to identify requirements for RFX4 and consequences of pathogenic mutation during human cortical development. We demonstrated that RFX4 restrains cortical neurogenesis in both 2-D and 3-D models and during both cortical excitatory (cEX) and inhibitory neuron (cIN) differentiation. While RFX transcription factors were previously assumed to behave as transcriptional activators (Harris et al. 2021; Choi et al. 2024), this work demonstrates a requirement for RFX4 to directly repress neuronal and synaptic gene expression during this process. We further found that both molecular and cellular phenotypes associated with RFX4 LOF in progenitors persist through neuronal differentiation, despite the cessation of RFX4 expression. RFX4 overexpression alone was insufficient to induce neuronal differentiation without concomitant or prior neuronal patterning; these results clarify prior conflicting studies suggesting that RFX4 could both stabilize neuronal progenitor production (Joung et al. 2023) and induce neuronal differentiation (Choi et al. 2024). Our work demonstrates that RFX4 is required repress neuronal gene expression to maintain the neuronal progenitor state, while LOF induces neurogenesis.

To investigate the mechanisms by which RFX4 regulates cortical neurogenesis, we identified endogenous genome-wide RFX4 binding during both cEX and cIN development, confirming the validity and quality of these data across multiple paradigms. We also identified other TFs that colocalized on the genome with RFX4 (e.g. TEAD1, RFX3) and tested whether these were affected by RFX4 LOF, to determine whether they could also act at RFX4-bound cis-regulatory elements (CREs) to regulate cortical neurogenesis. Specifically, we defined putative CREs that co-bound RFX4 and TEAD1; this was notable because TEAD TFs play known roles in regulating cortical neurogenesis (Mukhtar et al. 2020). Some of these co-bound CREs were associated with NOTCH pathway genes such as JAG1, congruent with the recent observation that TEAD transcription factors can modulate NOTCH signaling during mouse cortical neurogenesis (Perry et al. 2025).

Our data also demonstrated that RFX3 and RFX4 co-occupy CREs associated with synaptic genes and functionally interact to regulate gene expression, with RFX3 relying on RFX4 to bind most of these shared enhancers. Despite co-occupying putative CREs at synaptic genes, RFX3 and RFX4 requirements for cortical neuron development differ; RFX4 expression specifically during neurogenesis is required to represses neuronal gene expression, while RFX3 can activate later neuronal and synaptic gene expression during differentiation, a finding substantiated by Lai and colleagues using RFX3 LOF iGlut models (Lai et al. 2025). RFX3 was also previously shown to promote activity-dependent gene expression in cortical neurons through interactions with CREB1 (Lai et al. 2025; Neumann et al. 2025), versus the distinct role we describe here for RFX4 specifically in neural progenitors, suggesting distinct temporal and transcriptional activities for these TFs in cortical development. These divergent roles are congruent with the temporal restriction of RFX4 expression to progenitors, while RFX3 continues to be expressed in neurons (Wang et al. 2025). While our work here supports co-occupancy of RFX4 with TEAD1 or RFX3 at enhancers during cortical neurogenesis, future work is needed to further define the mechanistic relationships between the activities of these TFs and other TFs with enriched binding motifs under the RFX4 bound peaks we defined here.

We also used an unbiased drug screen to assess mechanisms of action that could reverse RFX4 LOF phenotypes, identifying functional interplay between RFX4 LOF and NOTCH signaling blockade. Specifically, we found that RFX4 functions downstream of NOTCH signaling and functionally cooperates with SOX2 and HES5 to regulate cortical neurogenesis. Our findings are congruent with a cooperative role for SOX2 in neuroectoderm and neural progenitor formation and maintenance (Graham et al. 2003; Bani-Yaghoub et al. 2006; Amador-Arjona et al. 2015; Batchuluun et al. 2017), while we also identified a previously undefined relationship between RFX4 and HES5, a NOTCH effector that, like RFX4, restrains neurogenesis (Ohtsuka et al. 2001; Bansod et al. 2017; Luiken et al. 2020). Our data indicate that RFX4 and HES5 activity are both required to cooperatively restrain neurogenesis and differentiation into early-born neurons, highlighting the importance of strict regulation of this process.

Examining the persisting consequences in neurons of altered neurogenesis resulting from RFX4 LOF, we found that these were specific to neurons which underwent a progenitor stage rather than being directly differentiated into iGluts. Similar findings have been reported for other NDD hPSC models (Schafer et al. 2019), supporting a developmental etiology involving disrupted neurogenesis for NDDs resulting from RFX4 mutation. Studies exploring other NDD-associated mutations have also reported altered cortical neurogenesis (Kaushik and Zarbalis 2016; Adam and Harwell 2020; Niu et al. 2024; Chapman et al. 2025; Kaushik et al. 2025; Prakasam et al. 2025) that can cause E/I functional neuron imbalance, a central hypothesis for the cellular etiology of NDDs (Siegel-Ramsay et al. 2021; Hollestein et al. 2023). For example, EZH1 LOF disrupts neurogenesis (Gracia-Diaz et al. 2023) while conditional Ezh2 knockout in mouse models enhances formation of TBR1+ and CTIP2+ neurons during peak cortical neurogenesis (Pereira et al. 2010). EZH2 has also been shown to act as an epigenetic barrier during neuronal differentiation of hPSC models (Ciceri et al. 2024). As mutations in each of these genes can cause NDDs, disruption of neurogenesis represents a critical developmental window sensitive to perturbation to cause NDDs.

Our cEX and cortical organoid models both exhibited precocious neurogenesis with persistent neuronal consequences, with LOF altering expression of lineage-specific neuronal markers. Interestingly, LOF in D-NPCs caused a persistent upregulation some TFs specific to cINs in cEXs, while the increase in FOXG1 immunopositivity in LOF organoid models may also indicate altered progenitor identity, as FOXG1 overexpression in organoids was previously reported to increase GABAergic neuron production (Mariani et al. 2015). Our observations of perturbed progenitor identity here are reminiscent of the altered dorsal-ventral brain patterning seen in Rfx4 knockout mouse and zebrafish models (Blackshear et al. 2003; Zhang et al. 2006; Ashique et al. 2009; Sedykh et al. 2018), suggesting that RFX4 mutations may affect both neurogenesis and neuronal lineage allocation.

Finally, having established requirements for RFX4 during cortical development, we examined how the pathogenic mutation p.R79C, a missense mutation in the DNA-binding domain predicted to act via LOF, affected regulation of cortical neurogenesis. Surprisingly, while this mutation largely abrogated RFX4 genome-wide binding like LOF models, it caused unique and substantial transcriptional changes, suggesting a distinct mechanism of pathogenicity. As RFX TFs can both homo- and heterodimerize (Morotomi-Yano et al. 2002) and can co-bind shared genomic targets, pathogenic mutation may alter these dynamics. Furthermore, it has been shown that two RFX family TFs can co-bind a single canonical X-box motif (Gajiwala et al. 2000), suggesting that RFX family TF heterodimerization may alter their transcriptional regulatory activity. Studying the basis of pathogenicity of additional mutations will be required to understand the etiology of RFX4-associated NDDs and underlying mechanisms. Together, this study elucidated previously unknown roles for and mechanisms of transcriptional repression by RFX4 during cortical neurogenesis, highlighting their disruption upon both LOF and pathogenic missense mutation and providing a necessary foundation to develop approaches for reversal of pathogenesis-associated phenotypes.

Methods

hPSC Model Generation and Culture

Work with human pluripotent stem cells (hPSCs) was performed under our approved Washington University Embryonic Stem Cell Research Office (ESCRO) under protocol #12-002. RFX4 heterozygous (HET) and homozygous (HOM) knockout hPSCs were generated in both the human embryonic stem cell (hESC) line WA09 and human induced pluripotent stem cell (hiPSC) line AN1.1 by targeting the first canonical exon (6) with CRISPR-Cas9-based genome engineering (Supplementary Fig. 1a). The same process was employed to generate RFX3 homozygous (RFX3-HOM) knockout AN1.1 hiPSC models by targeting exon 8 (Supplementary Fig. 5b). Finally, a patient-specific *RFX4* mutation (c.235C>T) was genetically engineered into the WA01 hESC line targeting one or both alleles of the *RFX4* gene with CRISPR-Cas9-based genome editing (Supplementary Fig. 6a). The validity of all models was confirmed by NGS-based amplicon sequencing (Sentmanat et al. 2018), with all model generation and validation conducted by the Washington University Genome Engineering & Stem Cell Center (GESC). All hPSCs were maintained under feeder-free conditions on vitronectin (Gibco™) coated plasticware in StemFlex Medium (Gibco™) at 37°C with 5% CO_2. Experiments were carried out between passages 15-60 for all hPSC lines. Details of cell backgrounds used for each experiment are detailed in Supplementary Data 20.

Modeling cortical inhibitory and excitatory neuron development

To model cortical inhibitory neuron development, we specified hPSCs as medial ganglionic eminence (MGE)-like progenitors with a ventral telencephalic progenitor (V-NPC, day 15) identity, as previously described (Meganathan et al. 2017) with minor modifications. Modeling of cortical excitatory neuron development was carried out as described in our prior work (Chapman et al. 2022; Chapman et al. 2024) by specifying hPSCs as progenitors with a dorsal telencephalic progenitor (D-NPC, day 20) identity and further differentiated into immature cortical excitatory neurons (cEXs, day 40). Induced glutamatergic-like neurons (iGluts) were generated by overexpressing the bHLH transcription factor Neurogenin-2 (NGN2) and as described in our prior work (Chapman et al. 2025) with cells constituting iGluts at day 21. For RFX4 overexpression experiments, wildtype hPSCs were transduced with an RFX4 open reading frame plasmid (Genecopoeia, H2578-Lv203) and cultured in neuronal media for 6 days before collection. Finally, to model 3-D human cortical development, dorsally patterned cortical organoids were generated as previously described (Lunn 2022) with minor modifications and collected on days 30 and 60. All protocols are detailed in Supplementary Materials.

Cellular Phenotyping

Changes in RFX4 in pathogenic and loss of function models was assessed by western blot and RT-qPCR using protein and RNA isolated from D-NPCs; similarly, changes in RFX3 was assessed by western blot and RT-qPCR using protein and RNA isolated from D-NPCs. Quantifications of neurosphere outgrowth were performed in both D-NPCs and V-NPCs after 12 days (D12) of differentiation and changes in immunopositive markers were assessed by immunocytochemistry 2 days after replating specified progenitors. Upon specification into progenitors, RT-qPCR was used to examine changes in gene expression in RFX4 HET LOF models. To examine interactions between SOX2, HES5, and RFX4, D-NPCs were treated with siRNAs on day 21 and collected on day 24; confirmation of siRNA knockdown and marker changes was assessed by RT-qPCR. To determine RFX4 protein function, luciferase assays were performed in WT and RFX4 HOM D-NPCs on day 24 after transfection of luciferase vectors. For our unbiased drug screen, we examined changes in OLIG2 immunopositivity in WT and HOM D-NPCs on day 24 after 4 days of treatment.

To determine changes in differentiation and proliferation in D-ORGs, immunocytochemistry was performed at days 30 (D30) and days 60 (D60). Examination of D-NPC RFX4-Bound genes was performed by RT-qPCR at day 40 of cEX and day 21 of iGlut differentiation; assessment of cortical layer and synaptic markers was performed similarly by RT-qPCR in day 40 cEXs. Finally, immunocytochemistry assessment of neuronal differentiation and synaptic production in monolayer cEXs was performed at day 40 and day 50, respectively. siRNA oligonucleotides are detailed in Supplementary Data 21. All RT-qPCR primers and antibodies used in this study are listed in Supplementary Data 22 and Supplementary Data 23, respectively. Details for luciferase oligonucleotides are listed in Supplementary Data 24. For detailed cellular phenotyping methods, see Supplementary Material.

RNA-sequencing and CUT&Tag

Both RNA-sequencing and CUT&Tag was performed as previously described (Chapman et al. 2024) on RFX4 LOF V-NPCs at day 15 and day 20 for RFX4 and RFX3 LOF and R79C D-NPCs. For NOTCH experiments, CUT&Tag for H3K4me and H3K27me3 in WT and RFX4 HOM D-NPCs was performed at day 24 following either DMSO or DAPT treatment; likewise, RNA-sequencing was performed in WT D-NPCs treated with either DMSO or DAPT on day 24. Finally, RNA-sequencing was performed on day 40 WT and RFX4 HOM cEXs. All raw data (RNA and CUT&Tag) is available from the Gene Expression Omnibus database under accession GSE316377. For full details on RNA-sequencing and CUT&Tag methodologies and data processing, see Supplementary Material.

Quantification and Statistical Analysis

Where appropriate, statistical analysis was carried out using a combination of tools available in GraphPad Prism version 9 (GraphPad Software; La Jolla, CA, USA, available from www.graphpad.com) or RStudio version 3.5.1 (RStudio: Integrated development environment for R; Boston, MA, USA. Available from www.rstudio.org). All technical replicates were averaged before statistical analysis and statistical tests used for the analysis of each data set are detailed in the figure legends or in the methods section for specific analysis paradigms including differential gene expression and differential binding analysis. A minimum of 3 independent differentiations (3 biological replicates) were used for each time point and biological condition with the number of differentiations used for each sample listed in the figure legends as N. The results in figures are presented as group mean +/- standard error (SE) indicating each biological replicate used for the analysis, unless otherwise specified in figure legends. Statistical significance is indicated with asterisks as follows: ns, not significant; ∗, $p<0.05$; ∗∗, $p<0.01$; ∗∗∗, $p<0.001$; ∗∗∗∗, $p<0.0001$ unless otherwise specified in figure legends.

Competing Interests

The authors declare no competing interests.

Acknowledgments

This work was supported by NIH Fellowship F31MH141956 to J.J.D., NIH Grants R01NS114551, R01MH124808, R01HD110556 to K.L.K., and by NIH P50HD103525 to Joseph Dougherty and Christina Gurnett (K.L.K. is project PI for the Human Cellular Models Unit of the Washington University Intellectual and Developmental Disabilities Research Center, with project effort funded by this grant). Foundations supporting this work included the Engelhart Family Foundation, Simons Foundation, M-CM Network, and pilot awards from the WU Hope Center, Center of Regenerative Medicine, and Institute for Clinical and Translational Sciences to K.L.K.

We would like to acknowledge the Washington University Genome Engineering & Stem Cell Center (GESC@MGI) for the generation of the genetically engineered induced human pluripotent stem cell lines used in this study. We further would like to acknowledge the Washington University Genome Technology Access Center (GTAC@MGI) for their work in sequencing RNA and Cut&Tag data. Finally, we would like to acknowledge the Washington University Human Cells, Tissue, and Organoids core (hCTO) for their work in generating early cortical organoid data.

Author Contributions

J.J.D. and K.L.K. designed the study. J.J.D. performed developmentally patterned differentiations and downstream cellular phenotyping for RFX4 LOF, RFX3 LOF, R79C, and NOTCH experiments. G.C. performed iGlut experiments. J.J.D. generated dorsally patterned organoids, G.C. cryo-sectioned organoids, and J.J.D. and G.C. performed immunocytochemistry on organoids. S.C. performed RFX4 overexpression experiments and RT-qPCR. F.B. performed R79C western blots. S.M. performed RT-qPCR and organoid immunocytochemistry. F.B. and H.J. generated immunofluorescence images. J.J.D. and G.C. performed bioinformatic analyses. W.B., C.V., S.E., and T.S.G. performed the drug screen to identify mechanisms of action for RFX4 LOF. M.S. and X.C. generated and confirmed validity of RFX3 KO hPSC lines. J.J.D. and G.C. analyzed data and generated figures. J.J.D. and K.L.K. wrote the manuscript and all authors approved the manuscript.

References

Adam MA, Harwell CC. 2020. Epigenetic regulation of cortical neurogenesis; orchestrating fate switches at the right time and place. *Curr Opin Neurobiol* **63**: 146-153.

Ajami N, Kerachian MA, Toosi MB, Ashrafzadeh F, Hosseini S, Robinson PN, Abbaszadegan MR. 2023. Inherited deletion of 9p22.3-p24.3 and duplication of 18p11.31-p11.32 associated with neurodevelopmental delay: Phenotypic matching of involved genes. *J Cell Mol Med* **27**: 496-505.

Albert M, Kalebic N, Florio M, Lakshmanaperumal N, Haffner C, Brandl H, Henry I, Huttner WB. 2017. Epigenome profiling and editing of neocortical progenitor cells during development. *EMBO J* **36**: 2642-2658.

Amador-Arjona A, Cimadamore F, Huang CT, Wright R, Lewis S, Gage FH, Terskikh AV. 2015. SOX2 primes the epigenetic landscape in neural precursors enabling proper gene activation during hippocampal neurogenesis. *Proc Natl Acad Sci U S A* **112**: E1936-1945.

Ashique AM, Choe Y, Karlen M, May SR, Phamluong K, Solloway MJ, Ericson J, Peterson AS. 2009. The Rfx4 transcription factor modulates Shh signaling by regional control of ciliogenesis. *Sci Signal* **2**: ra70.

Banerjee I, Senniappan S, Laver TW, Caswell R, Zenker M, Mohnike K, Cheetham T, Wakeling MN, Ismail D, Lennerz B et al. 2019. Refinement of the critical genomic region for congenital hyperinsulinism in the Chromosome 9p deletion syndrome. *Wellcome Open Res* **4**: 149.

Bani-Yaghoub M, Tremblay RG, Lei JX, Zhang D, Zurakowski B, Sandhu JK, Smith B, Ribecco-Lutkiewicz M, Kennedy J, Walker PR et al. 2006. Role of Sox2 in the development of the mouse neocortex. *Dev Biol* **295**: 52-66.

Bansod S, Kageyama R, Ohtsuka T. 2017. Hes5 regulates the transition timing of neurogenesis and gliogenesis in mammalian neocortical development. *Development* **144**: 3156-3167.

Batchuluun K, Azuma M, Fujiwara K, Yashiro T, Kikuchi M. 2017. Notch Signaling and Maintenance of SOX2 Expression in Rat Anterior Pituitary Cells. *Acta Histochem Cytochem* **50**: 63-69.

Blackshear PJ, Graves JP, Stumpo DJ, Cobos I, Rubenstein JL, Zeldin DC. 2003. Graded phenotypic response to partial and complete deficiency of a brain-specific transcript variant of the winged helix transcription factor RFX4. *Development* **130**: 4539-4552.

Cadwell CR, Bhaduri A, Mostajo-Radji MA, Keefe MG, Nowakowski TJ. 2019. Development and Arealization of the Cerebral Cortex. *Neuron* **103**: 980-1004.

Chapman G, Alsaqati M, Lunn S, Singh T, Linden SC, Linden DEJ, van den Bree MBM, Ziller M, Owen MJ, Hall J et al. 2022. Using induced pluripotent stem cells to investigate human neuronal phenotypes in 1q21.1 deletion and duplication syndrome. *Mol Psychiatry* **27**: 819-830.

Chapman G, Determan J, Edwards JR, Huettner JE, Crump S, Jetter H, Gabel HW, Kroll KL. 2025. TBRS-associated DNMT3A mutations disrupt cortical interneuron differentiation and neuronal networks. *bioRxiv*.

Chapman G, Determan J, Jetter H, Kaushik K, Prakasam R, Kroll KL. 2024. Defining cis-regulatory elements and transcription factors that control human cortical interneuron development. *iScience* **27**: 109967.

Choi W, Choe MS, Kim SM, Kim SJ, Lee J, Lee Y, Lee SM, Dho SH, Lee MY, Kim LK. 2024. RFX4 is an intrinsic factor for neuronal differentiation through induction of proneural genes POU3F2 and NEUROD1. *Cell Mol Life Sci* **81**: 99.

Cholfin JA, Rubenstein JL. 2007. Genetic regulation of prefrontal cortex development and function. *Novartis Found Symp* **288**: 165-173; discussion 173-167, 276-181.

Ciceri G, Baggiolini A, Cho HS, Kshirsagar M, Benito-Kwiecinski S, Walsh RM, Aromolaran KA, Gonzalez-Hernandez AJ, Munguba H, Koo SY et al. 2024. An epigenetic barrier sets the timing of human neuronal maturation. *Nature* **626**: 881-890.

Gajiwala KS, Chen H, Cornille F, Roques BP, Reith W, Mach B, Burley SK. 2000. Structure of the winged-helix protein hRFX1 reveals a new mode of DNA binding. *Nature* **403**: 916-921.

Gracia-Diaz C, Zhou Y, Yang Q, Maroofian R, Espana-Bonilla P, Lee CH, Zhang S, Padilla N, Fueyo R, Waxman EA et al. 2023. Gain and loss of function variants in EZH1 disrupt neurogenesis and cause dominant and recessive neurodevelopmental disorders. *Nat Commun* **14**: 4109.

Graham V, Khudyakov J, Ellis P, Pevny L. 2003. SOX2 functions to maintain neural progenitor identity. *Neuron* **39**: 749-765.

Harris HK, Nakayama T, Lai J, Zhao B, Argyrou N, Gubbels CS, Soucy A, Genetti CA, Suslovitch V, Rodan LH et al. 2021. Disruption of RFX family transcription factors causes autism, attention-deficit/hyperactivity disorder, intellectual disability, and dysregulated behavior. *Genet Med* **23**: 1028-1040.

Hollestein V, Poelmans G, Forde NJ, Beckmann CF, Ecker C, Mann C, Schafer T, Moessnang C, Baumeister S, Banaschewski T et al. 2023. Excitatory/inhibitory imbalance in autism: the role of glutamate and GABA gene-sets in symptoms and cortical brain structure. *Transl Psychiatry* **13**: 18.

Joung J, Ma S, Tay T, Geiger-Schuller KR, Kirchgatterer PC, Verdine VK, Guo B, Arias-Garcia MA, Allen WE, Singh A et al. 2023. A transcription factor atlas of directed differentiation. *Cell* **186**: 209-229 e226.

Kaushik G, Zarbalis KS. 2016. Prenatal Neurogenesis in Autism Spectrum Disorders. *Front Chem* **4**: 12.

Kaushik K, Chapman G, Prakasam R, Batool F, Saleh M, Determan J, Huettner JE, Kroll KL. 2025. Requirements for the neurodevelopmental disorder-associated gene ZNF292 in human cortical interneuron development and function. *Cell Rep* **44**: 115597.

Lai J, Demirbas D, Phillips K, Zhao B, Wallace H, Seferian M, Nakayama T, Harris H, Chatzipli A, Lee EA et al. 2025. Multi-omic analysis of the ciliogenic transcription factor RFX3 reveals a role in promoting activity-dependent responses via enhancing CREB binding in human neurons. *bioRxiv*.

Lui JH, Hansen DV, Kriegstein AR. 2011. Development and evolution of the human neocortex. *Cell* **146**: 18-36.

Luiken S, Fraas A, Bieg M, Sugiyanto R, Goeppert B, Singer S, Ploeger C, Warsow G, Marquardt JU, Sticht C et al. 2020. NOTCH target gene HES5 mediates oncogenic and tumor suppressive functions in hepatocarcinogenesis. *Oncogene* **39**: 3128-3144.

Lunn S. 2022. Development and application of human cortical organoids: A 1q21.1 study. in *School of Biosciences*. Cardiff University.

Mariani J, Coppola G, Zhang P, Abyzov A, Provini L, Tomasini L, Amenduni M, Szekely A, Palejev D, Wilson M et al. 2015. FOXG1-Dependent Dysregulation of GABA/Glutamate Neuron Differentiation in Autism Spectrum Disorders. *Cell* **162**: 375-390.

Meganathan K, Lewis EMA, Gontarz P, Liu S, Stanley EG, Elefanty AG, Huettner JE, Zhang B, Kroll KL. 2017. Regulatory networks specifying cortical interneurons from human embryonic stem cells reveal roles for CHD2 in interneuron development. *Proc Natl Acad Sci U S A* **114**: E11180-E11189.

Morotomi-Yano K, Yano K, Saito H, Sun Z, Iwama A, Miki Y. 2002. Human regulatory factor X 4 (RFX4) is a testis-specific dimeric DNA-binding protein that cooperates with other human RFX members. *J Biol Chem* **277**: 836-842.

Mukhtar T, Breda J, Grison A, Karimaddini Z, Grobecker P, Iber D, Beisel C, van Nimwegen E, Taylor V. 2020. Tead transcription factors differentially regulate cortical development. *Sci Rep* **10**: 4625.

Neumann S, Achiro JM, Watanabe M, Bonnano SL, Deng W, Wohlschlegel JA, Martin KC. 2025. Cytoplasmic and nuclear protein interaction networks of the synapto-nuclear messenger CRTC1 in neurons reveal cooperative chromatin binding between CREB1 and CRTC1, MEF2C and RFX3. *bioRxiv*.

Niu W, Yu S, Li X, Wang Z, Chen R, Michalski C, Jahangiri A, Zohdy Y, Chern JJ, Whitworth TJ et al. 2024. Longitudinal multi-omics reveals pathogenic TSC2 variants disrupt developmental trajectories of human cortical organoids derived from Tuberous Sclerosis Complex. *bioRxiv*.

Ohtsuka T, Sakamoto M, Guillemot F, Kageyama R. 2001. Roles of the basic helix-loop-helix genes Hes1 and Hes5 in expansion of neural stem cells of the developing brain. *J Biol Chem* **276**: 30467-30474.

Pereira JD, Sansom SN, Smith J, Dobenecker MW, Tarakhovsky A, Livesey FJ. 2010. Ezh2, the histone methyltransferase of PRC2, regulates the balance between self-renewal and differentiation in the cerebral cortex. *Proc Natl Acad Sci U S A* **107**: 15957-15962.

Perry CH, Lavado A, Thulabandu V, Ramirez C, Pare J, Dixit R, Mishra A, Yang J, Yu J, Cao X. 2025. TEAD switches interacting partners along neural progenitor lineage progression to execute distinct functions. *Genes Dev* **39**: 849-867.

Prakasam R, Determan J, Chapman G, Narasimhan M, Shen R, Saleh M, Kaushik K, Gontarz P, Meganathan K, Hakim B et al. 2025. Autism- and intellectual disability-associated MYT1L mutation alters human cortical interneuron differentiation, maturation, and physiology. *Stem Cell Reports* **20**: 102421.

Schafer ST, Paquola ACM, Stern S, Gosselin D, Ku M, Pena M, Kuret TJM, Liyanage M, Mansour AA, Jaeger BN et al. 2019. Pathological priming causes developmental gene network heterochronicity in autistic subject-derived neurons. *Nat Neurosci* **22**: 243-255.

Sedykh I, Keller AN, Yoon B, Roberson L, Moskvin OV, Grinblat Y. 2018. Zebrafish Rfx4 controls dorsal and ventral midline formation in the neural tube. *Dev Dyn* **247**: 650-659.

Sentmanat MF, Peters ST, Florian CP, Connelly JP, Pruett-Miller SM. 2018. A Survey of Validation Strategies for CRISPR-Cas9 Editing. *Sci Rep* **8**: 888.

Siegel-Ramsay JE, Romaniuk L, Whalley HC, Roberts N, Branigan H, Stanfield AC, Lawrie SM, Dauvermann MR. 2021. Glutamate and functional connectivity - support for the excitatory-inhibitory imbalance hypothesis in autism spectrum disorders. *Psychiatry Res Neuroimaging* **313**: 111302.

Vasan L, Moffat A, Mattar P, Schuurmans C. 2025. Neocortical neurogenesis: a proneural gene perspective. *FEBS J* **292**: 5580-5610.

Villalba A, Gotz M, Borrell V. 2021. The regulation of cortical neurogenesis. *Curr Top Dev Biol* **142**: 1-66.

Wang L, Wang C, Moriano JA, Chen S, Zuo G, Cebrian-Silla A, Zhang S, Mukhtar T, Wang S, Song M et al. 2025. Molecular and cellular dynamics of the developing human neocortex. *Nature*.

Xu P, Morrison JP, Foley JF, Stumpo DJ, Ward T, Zeldin DC, Blackshear PJ. 2018. Conditional ablation of the RFX4 isoform 1 transcription factor: Allele dosage effects on brain phenotype. *PLoS One* **13**: e0190561.

Zhang D, Stumpo DJ, Graves JP, DeGraff LM, Grissom SF, Collins JB, Li L, Zeldin DC, Blackshear PJ. 2006. Identification of potential target genes for RFX4_v3, a transcription factor critical for brain development. *J Neurochem* **98**: 860-875.

Zhang D, Zeldin DC, Blackshear PJ. 2007. Regulatory factor X4 variant 3: a transcription factor involved in brain development and disease. *J Neurosci Res* **85**: 3515-3522.

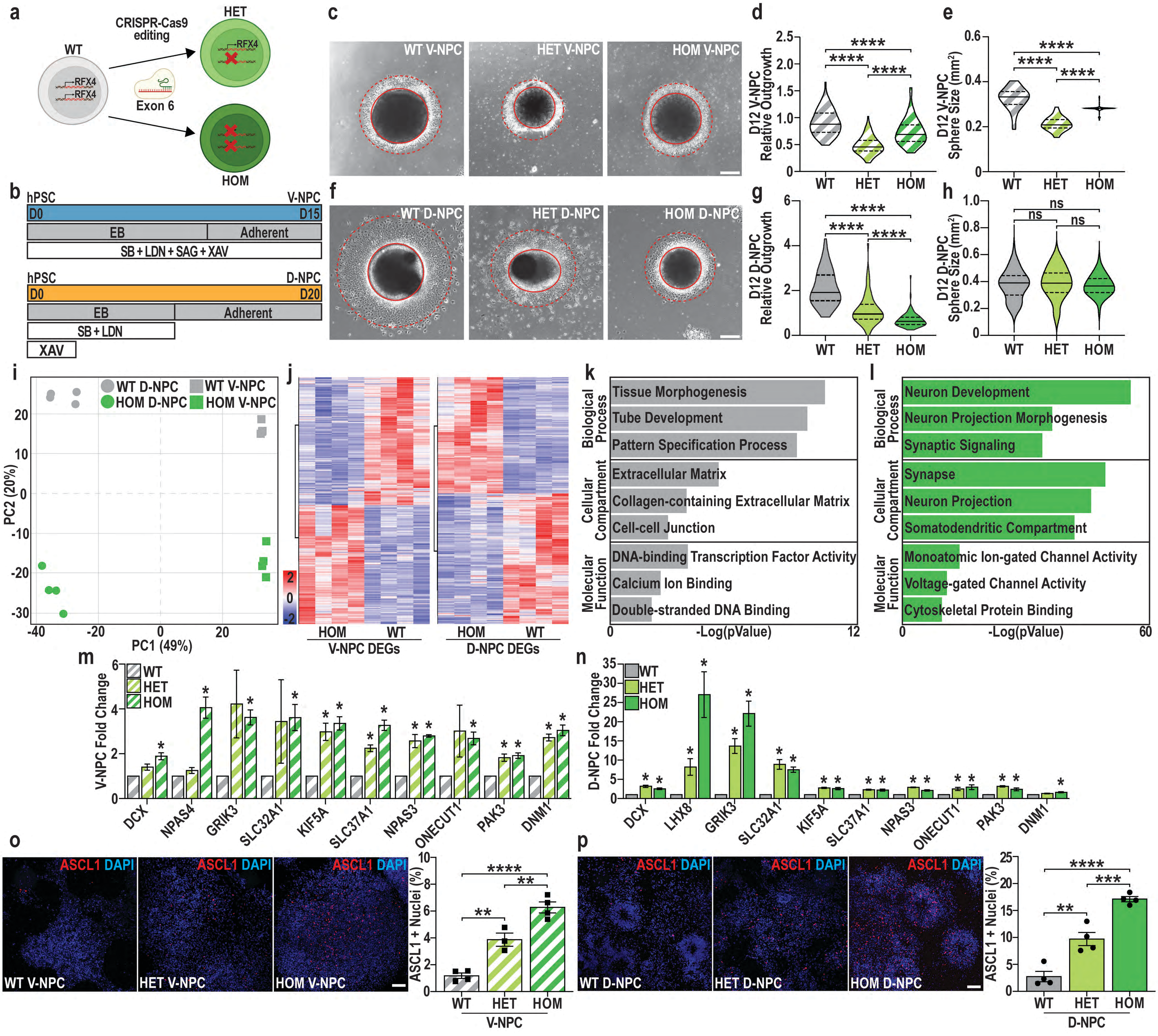

Fig. 1: Loss of RFX4 causes dosage-dependent induction of cortical neurogenesis.
(a-b) Schematic of **(a)** heterozygous (HET) and homozygous (HOM) RFX4 loss of function (LOF) hPSC model generation and **(b)** protocols used to specify hPSCs to ventral (V-) and dorsal (D-) neural progenitor cells (NPCs). **(c-h)** Quantification of **(c-e)** V-NPC and **(f-h)** D-NPC neurosphere outgrowth measuring **(d,g)** neuosphere body outgrowth (marked by dotted red circle) and **(e,h)** neurosphere size (marked by solid red circle) after 12 days of differentiation. **(i)** Principal component analysis (PCA), highlighting variation between WT D-NPCs (grey circles), RFX4 HOM D-NPCs (green circles), WT V-NPCs (grey squares), and RFX4 HOM V-NPCs (green squares). **(j)** Heatmaps of differentially expressed genes (DEGs) between WT and HOM V-NPCs (left) or D-NPCs (right). **(k-l)** Summary of gene ontology (GO) enrichment analysis for DEGs **(k)** downregulated or **(l)** upregulated by RFX4 LOF in both D- and V-NPCs. **(m-n)** RT-qPCR of genes significantly upregulated by RFX4 LOF; in WT, HET and HOM **(m)** V-NPCs and **(n)** D-NPCs. **(o-p)** Representative images and quantification of ASCL1 immunopositivity in **(o)** V-NPCs or **(p)** D-NPCs. Data are represented as **(d,e,g,h)** distributions with quartiles (dashed lines) and means (solid line) marked or **(d,e,g,h,m-p)** as mean +/- SEM, with **(m-p)** fold change calculated relative to GAPDH. Data in **(d,e,g,h)** was analyzed using one-way ANOVA (n=4) or **(m-n)** Student's t-test (n=4); ns = not significant, *p<0.05, **p<0.01, ***p<0.001, and ****p<0.0001, scale bars = **(c,f)** 100 µm and **(o,p)** 50 µm.

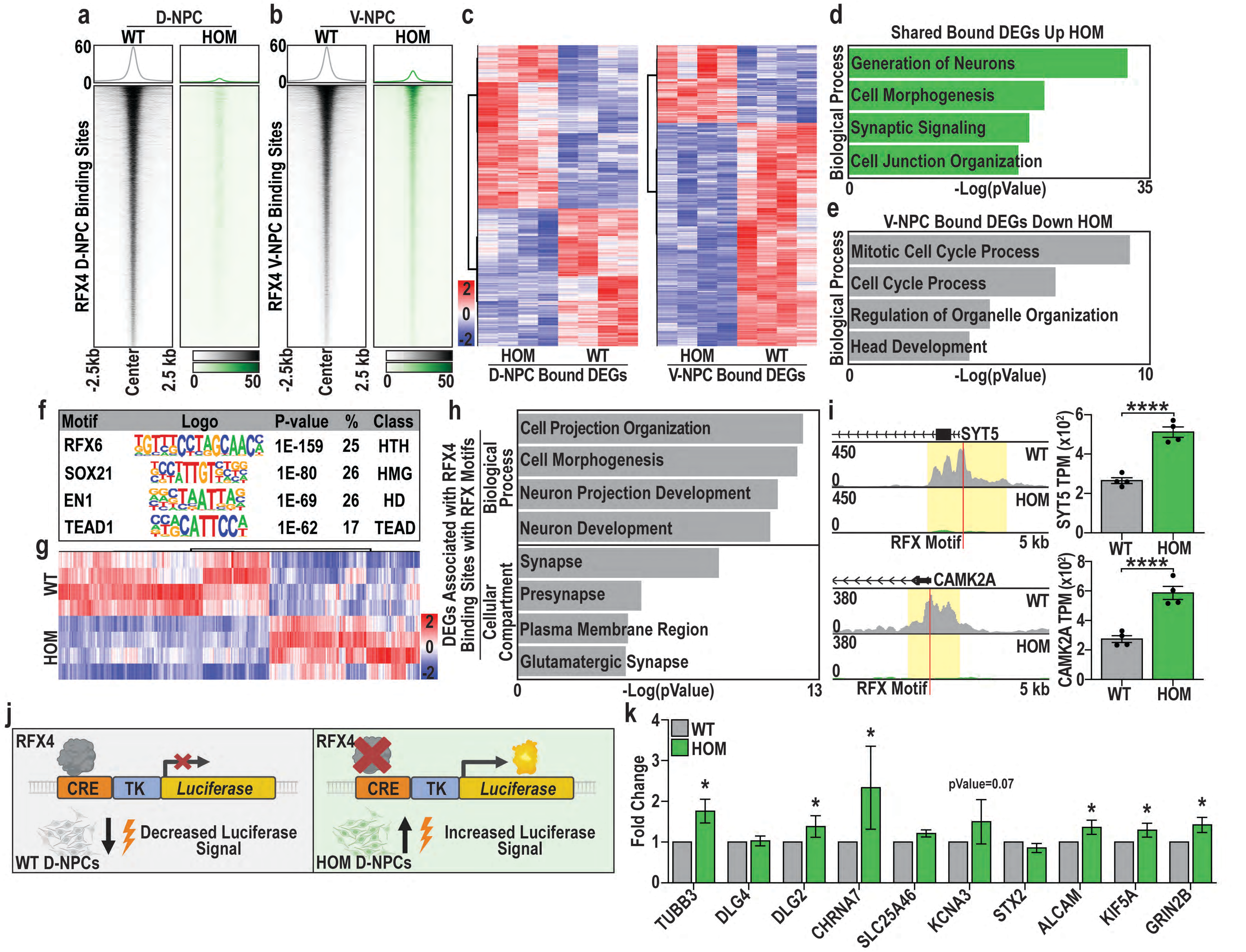

Fig. 2: RFX4 directly restrains the onset of neuronal and synaptic gene expression.

(a-b) Heatmaps of all RFX4 bound sites in WT and HOM **(a)** D-NPCs and **(b)** V-NPCs. **(c)** Heatmaps of DEGs associated with RFX4 binding (bound DEGs) in D-NPCs (left) and V-NPCs (right). **(d-e)** Summary of GO enrichment analysis for bound DEGs **(d)** upregulated in HOM V- and D-NPCs or **(e)** downregulated in HOM V-NPCs. **(f)** Summary of transcription factor binding site (TFBS) enrichment analysis of RFX4 bound DEGs. **(g)** Heatmap of RFX4 D-NPC bound DEGs associated with an RFX TFBS. **(h)** Summary of GO enrichment analysis for RFX4 bound DEGs associated with an RFX TFBS. **(i)** Examples of RFX4 D-NPC bound DEGs containing an RFX TFBS. **(j)** Experimental scheme and model for testing the hypothesized regulatory relationship between RFX4 and neuronal gene expression using luciferase assays. **(k)** Relative fold change in luciferase signal in HOM D-NPCs relative to the WT control. Data is represented as **(i,k)** mean +/- SEM and was analyzed by **(i)** differential gene expression analysis (n=4), or **(k)** Student's t-test (n≥3); **(i,k)** ns = not significant, *p<0.05 and ****p<0.0001.

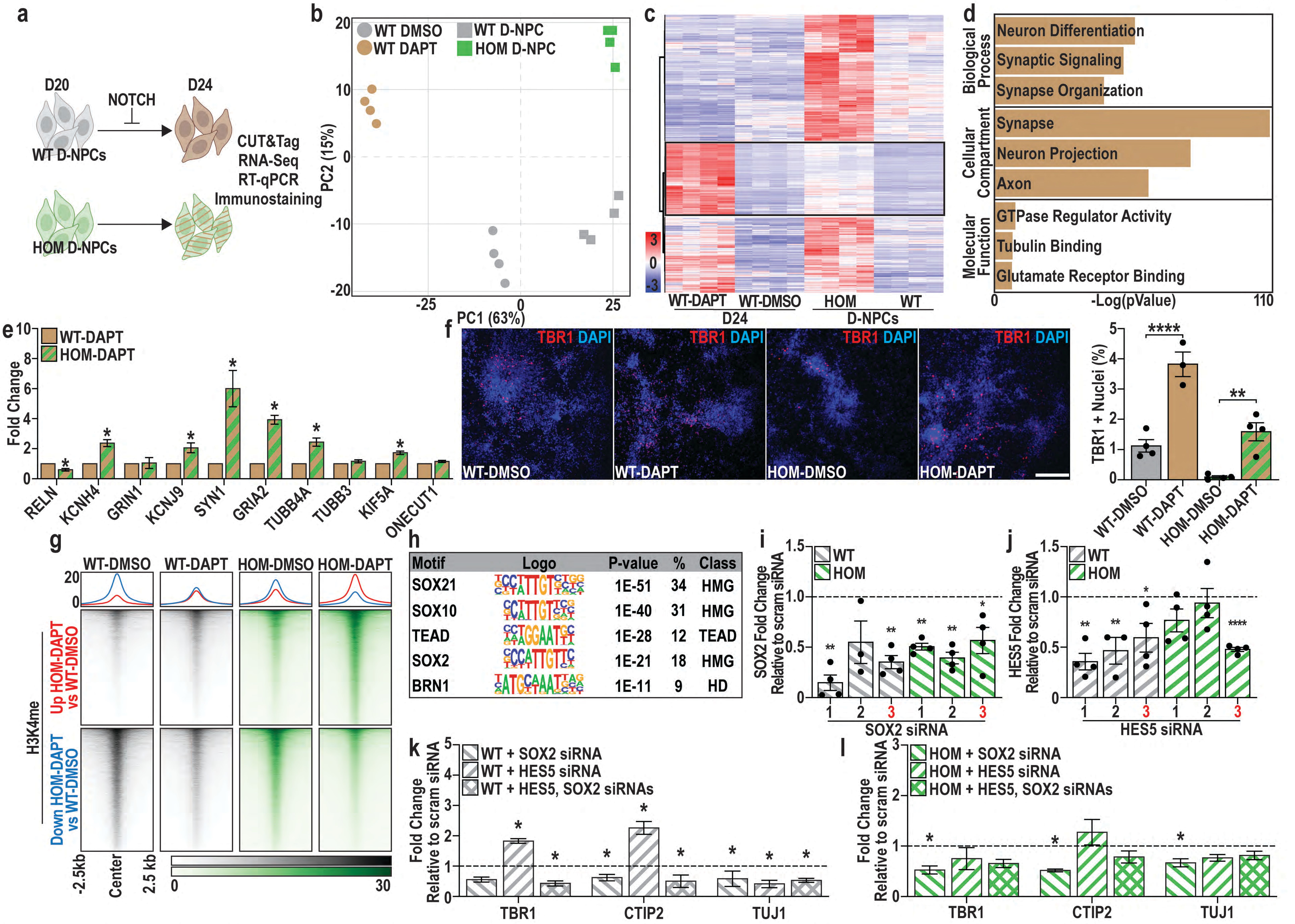

Motif	Logo	P-value	%	Class
SOX21		1E-51	34	HMG
SOX10		1E-40	31	HMG
TEAD		1E-28	12	TEAD
SOX2		1E-21	18	HMG
BRN1		1E-11	9	HD

Fig. 3: RFX4 regulates the onset of cortical neurogenesis downstream of NOTCH signaling.

(a) Schematic of experimental approach for assessing the effect of NOTCH inhibition (using DAPT) on WT and RFX4 HOM D-NPCs. **(b)** PCA highlighting variation between, WT-DMSO vehicle treated D-NPCs (grey circles), WT-DAPT treated D-NPCs (brown circles), and untreated WT D-NPC (grey squares), and RFX4 HOM D-NPCs (green squares). **(c)** Heatmap of RFX4 HOM DEGs, highlighting similar gene expression increases upon DAPT treatment, with genes upregulated most strongly by NOTCH inhibition indicated (black rectangle). **(d)** Summary of GO enrichment analysis of genes upregulated by RFX4 LOF and further upregulated by NOTCH inhibition (black rectangle from c). **(e)** RT-qPCR of genes significantly upregulated by RFX4 LOF and further upregulated by NOTCH inhibition in WT-DAPT and HOM-DAPT cells. **(f)** Representative images and quantification of TBR1 immunopostitivity in WT-DMSO, WT-DAPT, RFX4 HOM-DMSO, and RFX4 HOM-DAPT treated D-NPCs, highlighting a significant effect of DAPT treatment in both WT and HOM D-NPCs ($F_{1,11}$=69.41). **(g)** Heatmap of H3K4me sites upregulated (top, red) or downregulated (bottom, blue) in RFX4 HOM-DAPT D-NPCs versus WT-DMSO D-NPCs. **(h)** Summary of TFBS enrichment analysis for H3K4me sites lost upon NOTCH inhibition in D-NPCs. **(i-j)** RT-qPCR quantification of **(i)** SOX2 mRNA or **(j)** HES5 mRNA expression levels in WT and HOM D-NPCs treated with SOX2 or HES5 siRNAs respectively, relative to scram siRNA control treated D-NPCs (red text indicates siRNA used for subsequent experiments). **(k-l)** RT-qPCR for neuronal markers in **(k)** WT or **(l)** HOM D-NPCs treated with SOX2 and/or HES5 siRNAs. Data are represented as **(e,f,i-l)** mean +/- SEM, with fold change calculated relative to **(e)** GAPDH or **(i-l)** RPL30. Data was analyzed by **(e,i-l)** Student's t-test (n=4) or **(f)** two-way ANOVA (n=4); ns = not significant, *p<0.05, **p<0.01, and ****p<0.0001, scale bar = 100 µm.

Determan_Fig. 4

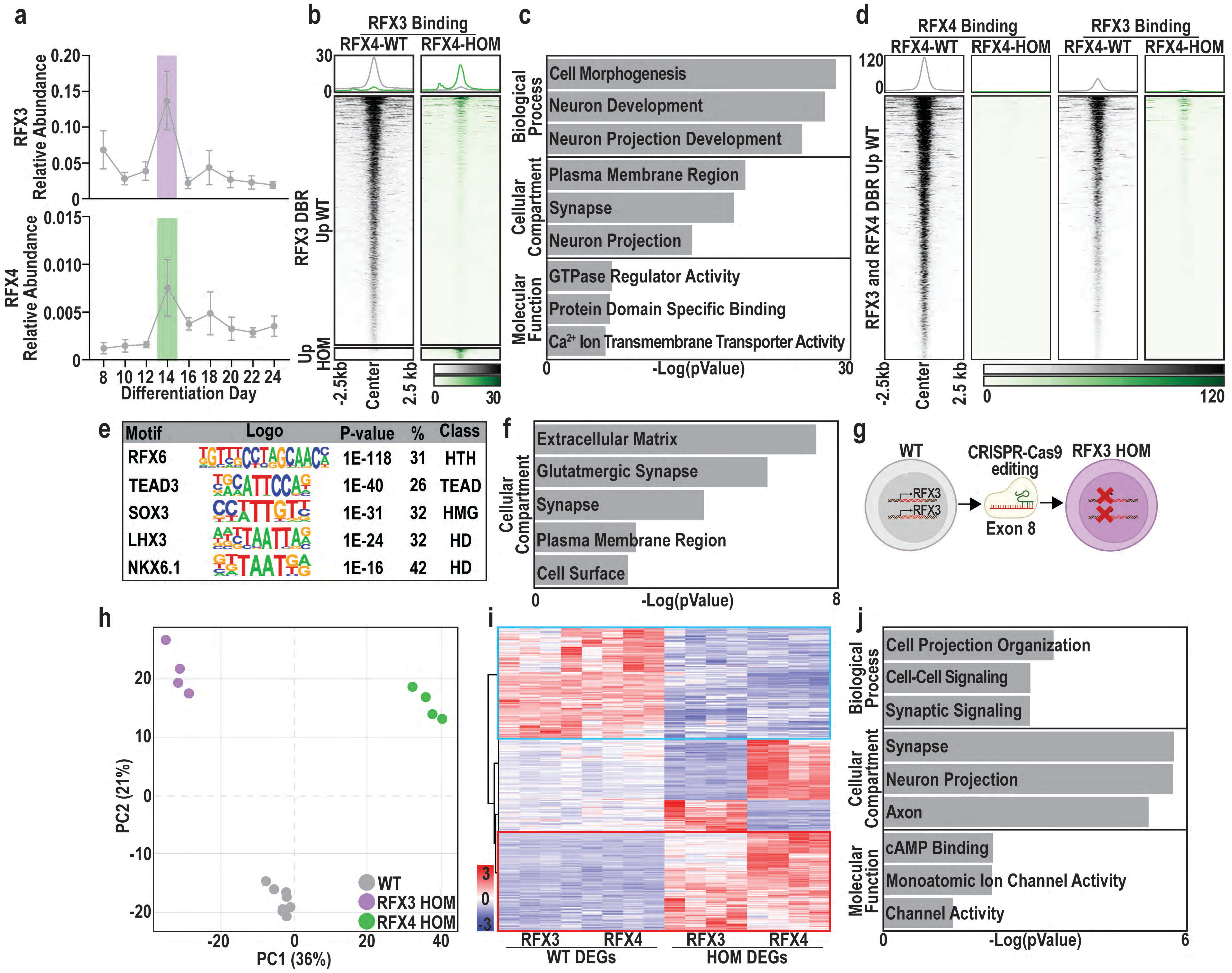

Fig. 4: RFX3 binding is contingent on RFX4 but plays a unique neurodevelopmental role. **(a)** RT-qPCR quantifying RFX3 (top, purple) and RFX4 (bottom, green) mRNA expression levels from day 8-24 of WT D-NPC differentiation, with peak expression highlighted. **(b)** Heatmap of RFX3 binding in RFX4 WT and HOM D-NPCs, separating sites which lost (upper panel) or gained (lower) RFX3 binding in response to RFX4 LOF. **(c)** Summary of GO enrichment analysis for genes associated with an RFX3 bound site lost in RFX4 HOM D-NPCs. **(d)** Heatmaps of RFX3 and RFX4 binding for co-bound sites that lose RFX4 binding in RFX4 HOM D-NPCs. **(e)** Summary of TFBS enrichment analysis for RFX3/4 co-bound sites at which binding is lost in RFX4 HOM D-NPCs. **(f)** Summary of GO enrichment analysis of RFX4 DEGs that are associated with RFX3/4 co-bound sites lost in RFX4 HOM D-NPCs. **(g)** Schematic of homozygous (HOM) RFX3 loss of function (LOF) hPSC model generation. **(h)** PCA plot highlighting variation in gene expression between WT (grey circles), RFX3 HOM (purple circles), and RFX4 HOM (green circles) D-NPCs. **(i)** Heatmap of DEGs dysregulated upon both RFX3 LOF or RFX4 LOF, with genes similarly downregulated or upregulated in both RFX3 and RFX4 HOM models highlighted (blue and red boxes, respectively). **(j)** Summary of GO enrichment analysis for DEGs downregulated upon RFX3 LOF. Data represents **(a)** mean +/- SEM, with fold change calculated relative to GAPDH.

Determan_Fig. 5

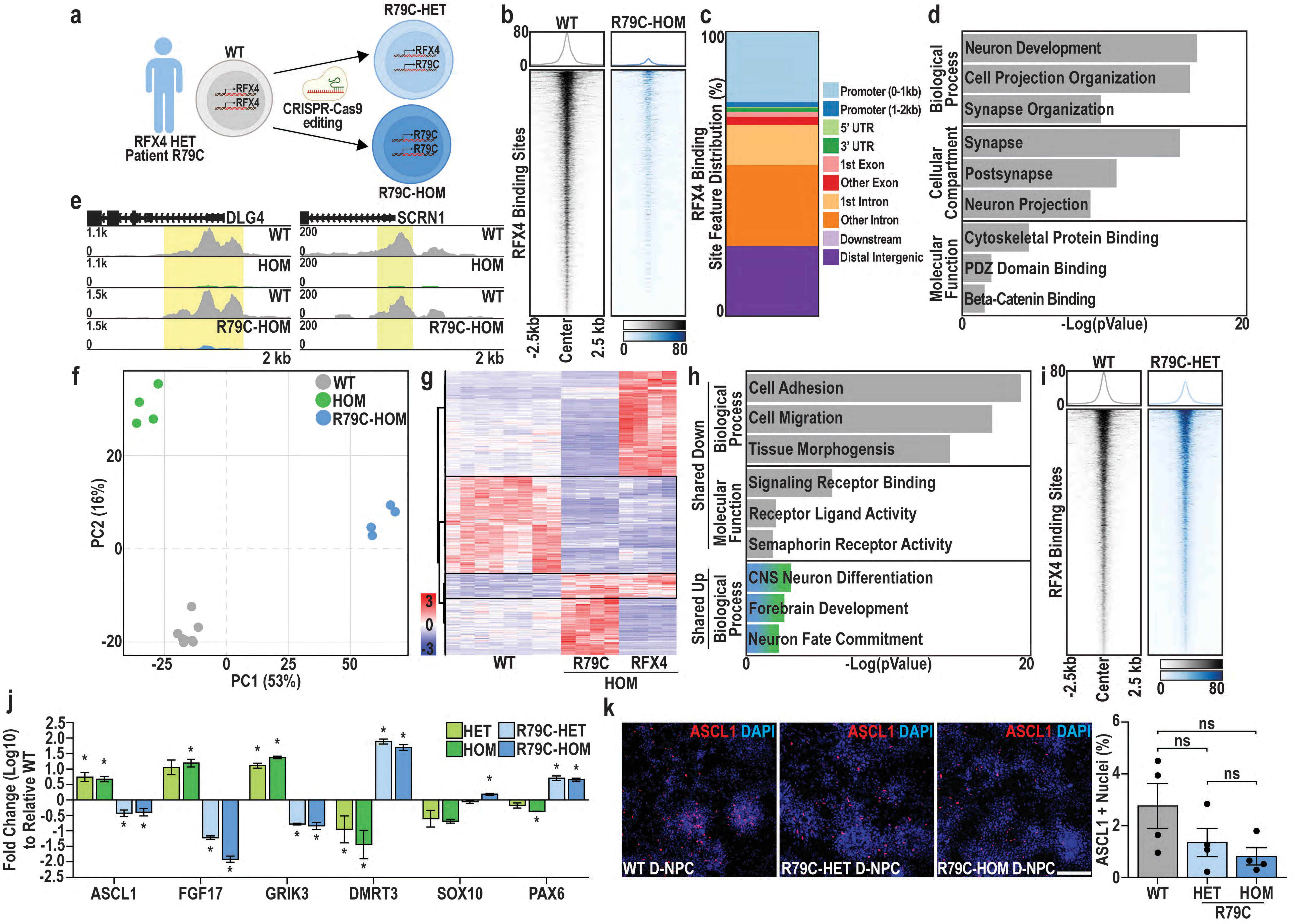

Fig. 5: Pathogenic RFX4 missense mutation disrupts genome-wide binding, but has distinct effects from LOF on transcriptional regulation.

(a) Variant knock-in of a heterozygous (R79C-HET) or homozygous (R79C-HOM) RFX4 missense mutation into WT hPSCs to model RFX4 pathogenic mutation. **(b)** Heatmap of RFX4 binding in WT and R79C-HOM D-NPCs. **(c)** Distribution of RFX4 binding sites relative to key genomic features. **(d)** Summary of GO enrichment analysis for genes associated with RFX4 binding sites lost in R79C-HOM D-NPCs. **(e)** Examples of RFX4 binding in browser track views, highlighting similar losses in RFX4 HOM and R79C-HOM D-NPCs at two genes. **(f)** PCA plots highlighting distinct alterations in gene expression between the WT control (grey circles), RFX4 HOM (green circles), and R79C-HOM (blue circles) D-NPCs. **(g)** Heatmap of DEGs dysregulated upon RFX4 LOF and pathogenic mutation, highlighting genes similarly dysregulated by both perturbations (black boxes). **(h)** Summary of GO enrichment analysis for DEGs downregulated (top, grey) or upregulated (bottom, blue/green) in both R79C-HOM and RFX4 HOM D-NPCs. **(i)** Heatmap of RFX4 bound sites associated with R79C-HET D-NPCs DEGs. **(j)** RT-qPCR for a selection of R79C-HOM and RFX4 HOM DEGs that showed opposing gene expression changes across the LOF and pathogenic mutant HET and HOM models. **(k)** Representative images and quantification of the ASCL1 immunopositivity in WT, R79C-HET and -HOM D-NPCs. Data are represented as **(j,k)** mean +/- SEM with fold changes calculated relative to RPL30. Data was analyzed by **(j)** Student's t-test (n=4) or **(k)** one-way ANOVA (n=4); ns = not significant and *p<0.05. **(k)** Scale bar = 50 μm.

Determan_Fig. 6

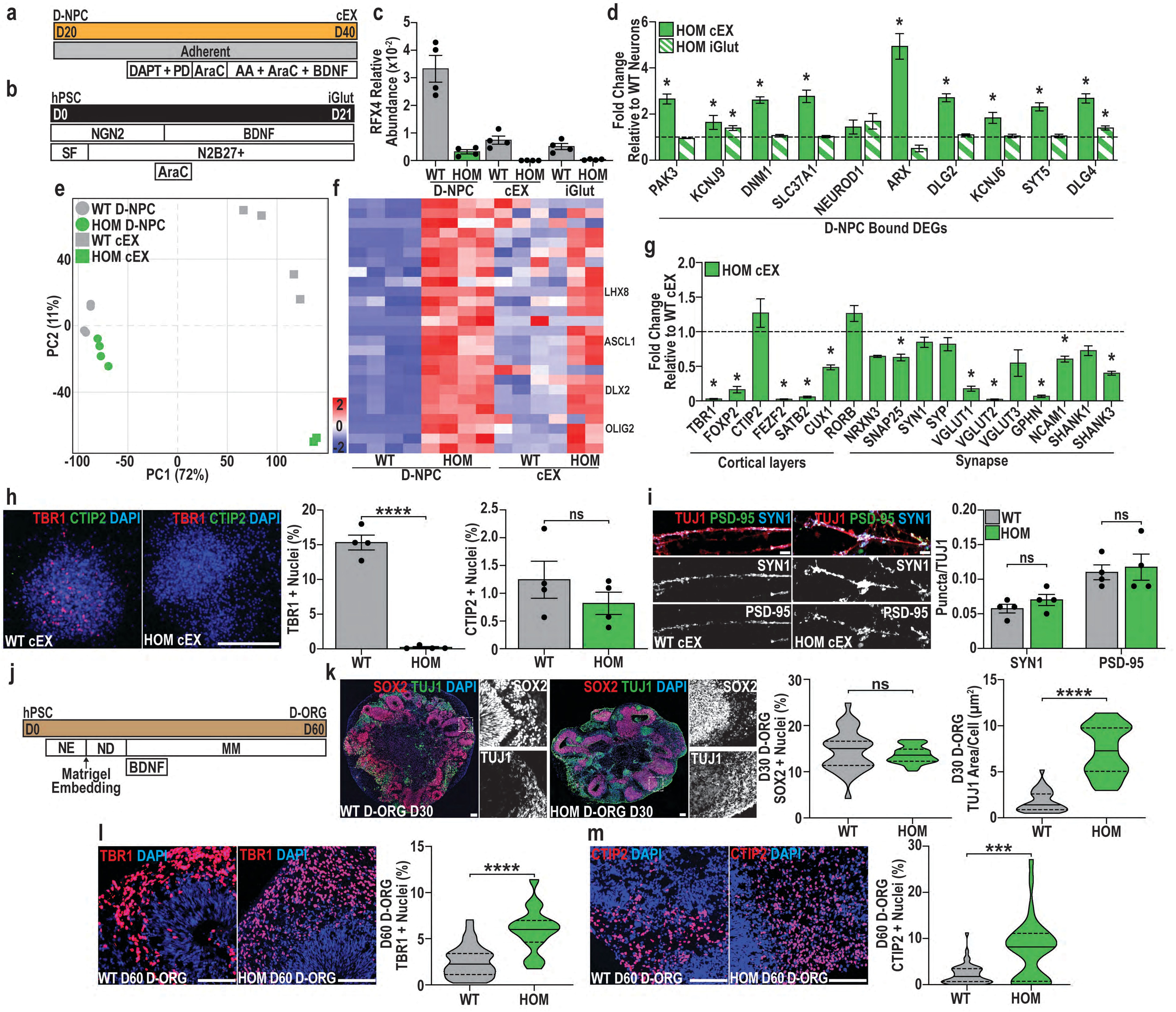

Fig. 6: RFX4 expression during neurogenesis is necessary for stratification of neuronal layers in cortical organoids. **(a-b)** Differentiation schematic for generating **(a)** cortical excitatory neurons (cEXs) and **(b)** glutamatergic-like neurons (iGluts). **(c)** RT-qPCR of RFX4 mRNA expression in WT and HOM D-NPCs, cEXs, and iGluts relative to RPL30 endogenous control, highlighting restriction of RFX4 expression to D-NPCs. **(d)** RT-qPCR for a selection of RFX4 D-NPC bound DEGs upregulated in RFX4 HOM D-NPCs, showing fold change in expression across RFX4 HOM cEXs and iGluts relative to expression levels in the corresponding WT cells. **(e)** PCA plot highlighting an increased divergence between the transcriptomic profiles of WT (grey) and HOM (green) cEXs (squares) versus D-NPCs (circles). **(f)** Heatmap of transcription factors upregulated upon RFX4 LOF in both D-NPCs and cEXs. **(g)** RT-qPCR for cortical layer and synaptic markers in HOM cEXs relative to WT cEXs. **(h-i)** Representative images and quantification of **(h)** TBR1 and CTIP2 immunopositivity and **(i)** PSD-95+ and SYN1+ puncta localized to TUJ1 immunopositive neurites in WT and HOM cEXs. **(j)** Schematic of the protocol used to generate dorsal cortical organoids (D-ORG). **(k-m)** Representative images and quantification of **(k)** SOX2 immunopositivity and the area of TUJ1 immunopositivity in D30 D-ORGs and **(l)** TBR1 and **(m)** CTIP2 immunopositivity in D60 D-ORGs. Data is represented as **(c,d,g-i)** mean +/- SEM, with fold changes calculated relative to RPL30, or **(k-m)** as data distributions with quartiles (dashed lines) and median (solid line) marked. Data was analyzed by **(d,g-i)** Student's t-test (n=4) or **(k-m)** Mann-Whitney test (n≥12); ns = not significant, *p<0.05, ***p<0.001, and ****p<0.0001. Scale bars = **(h,i)** 200 µm or **(k-m)** 100 µm.